Eur. Phys. J. A **8**, 205–216 (2000)

THE EUROPEAN PHYSICAL JOURNAL A

Effect of the entrance channel on the synthesis of superheavy elements

G. Giardina[1], S. Hofmann[2], A.I. Muminov[3], and A.K. Nasirov[3,4,a]

[1] Istituto Nazionale di Fisica Nucleare, Sezione di Catania, and Dipartimento di Fisica dell'Università di Messina, 98166 Messina, Italy
[2] Gesellschaft für Schwerionenforschung, Darmstadt, Germany
[3] Heavy Ion Physics Department, Institute of Nuclear Physics, Tashkent, Uzbekistan
[4] Bogoliubov Laboratory of the Theoretical Physics, JINR, 141980, Dubna

Received: 15 December 1999
Communicated by P. Schuck

Abstract. Cross-sections for the synthesis of superheavy elements were analyzed using the concept of a dinuclear system. Experimental values for the production of elements $Z = 104, 108, 110, 111$ and 112 by *cold fusion reactions* with targets of ^{208}Pb and ^{209}Bi were reproduced. The model reveals the importance of entrance channel dynamics and competition between quasi-fission and complete fusion processes. Energy windows were observed which allow capture of the reacting nuclei and formation of the compound nucleus. The quantities were studied which are significant for the interaction dynamics of massive nuclei in the entrance channel.

PACS. 24.10.-i Nuclear-reaction models and methods – 25.60.Pj Fusion reactions – 25.70.Jj Fusion and fusion-fission reactions

1 Introduction

The measured excitation functions of evaporation residues in the synthesis of elements from the $Z = 104$ to $Z = 112$ show that the cross-section and the energy window in which the events were observed [1] tend to decrease sharply. The dinuclear system (DNS) concept allows a description of the cross-sections in *cold* and *hot* fusion reactions and an implicit estimation of the competition between complete fusion and quasi-fission processes [2–4]. Calculations based on the DNS-concept show that entrance channel effects are important to describe the experimental data in the case of collisions of massive nuclei. The aim of this paper is to establish these effects and to analyse the role of the intrinsic fusion barrier, the quasi-fission barrier, the excitation energy of both the dinuclear system and the compound nucleus. As a result we obtained a beam energy window for the capture of the nuclei before the system will fuse.

Using combined dynamical and statistical approaches [5,6] the excitation functions of fusion and of evaporation residue yield were calculated for reactions of {^{50}Ti, ^{58}Fe, ^{64}Ni, ^{70}Zn} projectiles and {^{208}Pb, ^{209}Bi} targets resulting in the elements with proton number Z =104, 108, 110, 111, 112 and 113. We compare the calculated cross-sections with the data of experiments conducted at GSI Darmstadt, Germany, for the same reactions. We also extend our calculations for the synthesis of the superheavy element $Z = 114$ using the ^{76}Ge + ^{208}Pb reaction. The paper is organized as follows: the basic formalism is presented in Section 2; the results are discussed in Section 3; the summary is given in Section 4.

2 Theoretical method

In the dinuclear system concept [2] the evaporation residue cross-section is factorized as follows:

$$\sigma_{\rm er}(E) = \sum_{\ell=0}^{\infty}(2\ell+1)\sigma_{\ell}^{\rm fus}(E,\ell)W_{\rm sur}(E,\ell), \qquad (1)$$

where the entrance channel effects are included in the partial fusion cross-section $\sigma_{\ell}^{\rm fus}(E)$ defined by the expressions:

$$\sigma_{\ell}^{\rm fus}(E) = \sigma_{\ell}^{\rm capture}(E)P_{\rm CN}(E,\ell), \qquad (2)$$

$$\sigma_{l}^{\rm capture}(E) = \frac{\lambda^2}{4\pi}\mathcal{P}_{\ell}^{\rm capture}(E). \qquad (3)$$

Here λ is the de Broglie wavelength of the entrance channel, $P_{\rm CN}(E,\ell)$ is a factor taking into account the decrease of the fusion probability due to break up of the dinuclear system before fusion, $\mathcal{P}_{\ell}^{\rm capture}(E)$ is the capture probability which depends on the collision dynamics and determines the amount of partial waves leading to capture. The

[a] e-mail: nasirov@thsun1.jinr.ru

number of the partial waves was obtained by solving the equation of motion for the relative distance and orbital angular momentum

$$\mu(R(t))\,\ddot{\mathbf{R}} + \gamma_R(R(t))\,\dot{\mathbf{R}}\,(t) = -\frac{\partial V(R(t))}{\partial R}, \qquad (4)$$

$$\frac{\mathrm{d}L}{\mathrm{d}t} = \gamma_\theta(R(t))\left(\dot{\theta}R_{\mathrm{eff}}^2 - \dot{\theta}_1 R_{1\mathrm{eff}}^2 - \dot{\theta}_2 R_{2\mathrm{eff}}^2\right), \qquad (5)$$

where $R(t)$ is the relative motion coordinate, $\dot{\mathbf{R}}\,(t)$ is the corresponding velocity; $\dot{\theta}$, $\dot{\theta}_1$ and $\dot{\theta}_2$ are angular velocities of the dinuclear system and its fragments, respectively; γ_R and γ_θ are the friction coefficients of relative motion along R and tangential motion when two nuclei roll on each other's surfaces, respectively; $V(R)$ is the nucleus-nucleus potential; $\mu(R(t))$ is the reduced mass of the system; R_1 and R_2 are the fragment radii;

$$R_{\mathrm{eff}} = \frac{R + R_1 + R_2}{2}, \qquad R_{1(2)\mathrm{eff}} = \frac{R_{1(2)}}{R_1 + R_2}R,$$

where $R_{1(2)}$ is the nucleus radius (see expression (A.6) in Appendix A). The friction coefficients $\gamma_R(\gamma_\theta)$ and a change $\delta V(R)$ of the nucleus-nucleus potential during the interaction time t,

$$V(R(t)) = V_0(R(t)) + \delta V(R), \qquad (6)$$

are calculated from the estimation of the coupling term between the relative motion of nuclei and the intrinsic excitation of nuclei [5]. The explicit expressions for them are presented in Appendix A.

The nucleus-nucleus potential includes Coulomb, nuclear, and rotational potentials:

$$V_0(\mathbf{R}) = V_{\mathrm{C}}(\mathbf{R}) + V_{\mathrm{nucl}}(\mathbf{R}) + V_{\mathrm{rot}}(\mathbf{R}) \qquad (7)$$

(details are in Appendix A). In the calculations we took into account the dynamic contribution $\delta\mu(R)$ to the reduced mass

$$\mu(R) = \delta\mu(R) + m_0 A_{\mathrm{T}} A_{\mathrm{P}}/A_{\mathrm{tot}} \times \left(1 - \frac{2}{A_{\mathrm{tot}}}\int \frac{\rho_1^{(0)}(\mathbf{r}-\mathbf{r_1})\rho_2^{(0)}(\mathbf{r}-\mathbf{r_2})}{\rho_1^{(0)}(\mathbf{r}-\mathbf{r_1}) + \rho_2^{(0)}(\mathbf{r}-\mathbf{r_2})}\mathrm{d}^3\mathbf{r}\right), \qquad (8)$$

where $A_{\mathrm{tot}} = A_{\mathrm{T}} + A_{\mathrm{P}}$, $\rho_1^{(0)}$ and $\rho_2^{(0)}$ are nucleon densities of the dinuclear system fragments (details are in Appendix B); $\mathbf{r_1}$ and $\mathbf{r_2}$ are coordinates of the fragment centers-of-mass; m_0 is the nucleon mass; A_{T} and A_{P} are mass number of the target- and projectile-nucleus, respectively.

Calculations showed that use of these kinetic coefficients leads to gradual dissipation of kinetic and rotational energy [5]. It was shown that at collisions of massive nuclei despite of continuous dissipation the capture becomes impossible at larger values of beam energy than the Coulomb barrier, because of the small size of the well in the nucleus-nucleus potential. The dissipation is not sufficient to trap colliding nuclei in the potential well to create a necessary condition for fusion. In this case

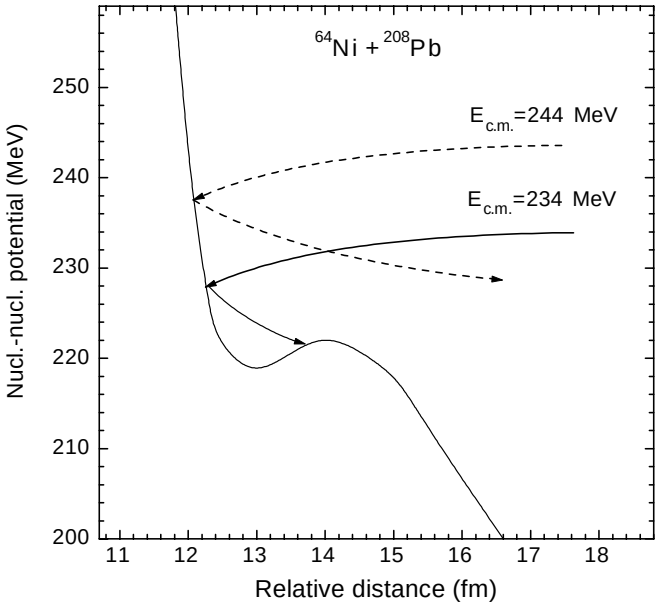

Fig. 1. Dependence of capture (solid curve) and quasi-fission (dashed curve) processes for nucleus-nucleus collisions on the internuclear potential $V(R)$ and on the initial values of the beam energy $E_{\mathrm{c.m.}}$.

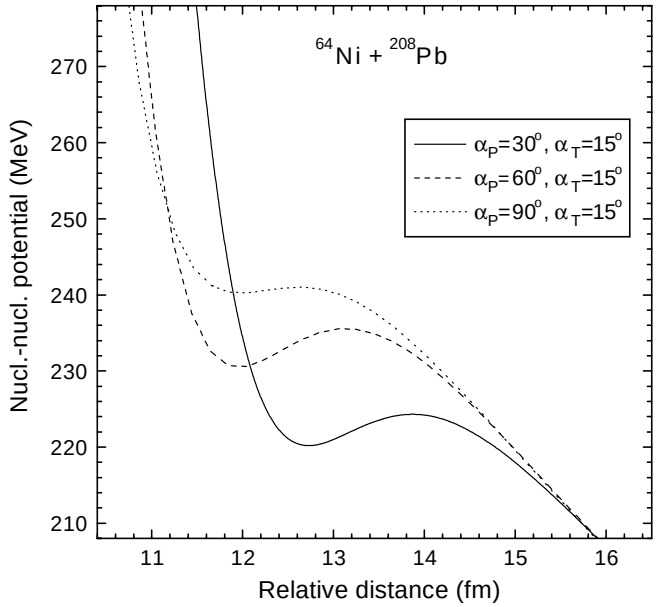

Fig. 2. Dependence of the nucleus-nucleus potential on the mutual orientation of colliding nuclei; solid line: $\alpha_1 = 30^\circ$ and $\alpha_2 = 15^\circ$; dashed line: $\alpha_1 = 60^\circ$ and $\alpha_2 = 15^\circ$; dotted line: $\alpha_1 = 90^\circ$ and $\alpha_2 = 15^\circ$. The angles α_1 and α_2 are defined in fig. 3.

the formed dinuclear system undergoes quasi-fission (see sketch in fig. 1). The nucleus-nucleus potential $V(R)$ depends on the mutual orientations of the symmetry axes of deformed nuclei relative to $\mathbf{R}(t)$ (fig. 2). The quadrupole (2^+) and octupole (3^-) collective excitations in spherical nuclei are taken into account. Thus, it is possible to consider fusion at different initial orientations of the symme-

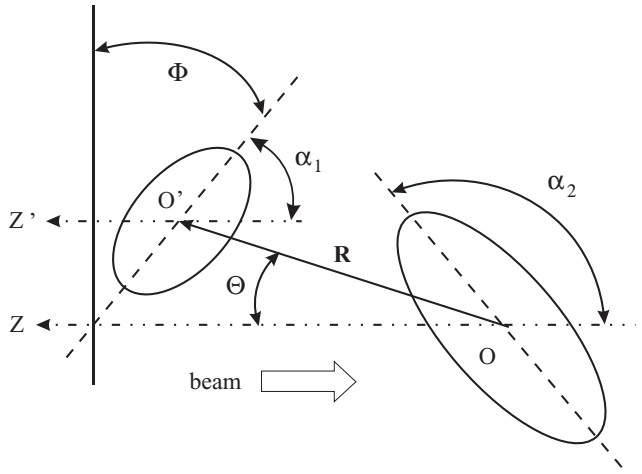

Fig. 3. The coordinate systems and angles which were used for the description of the initial orientations of projectile and target nuclei. The beam direction is opposite to OZ.

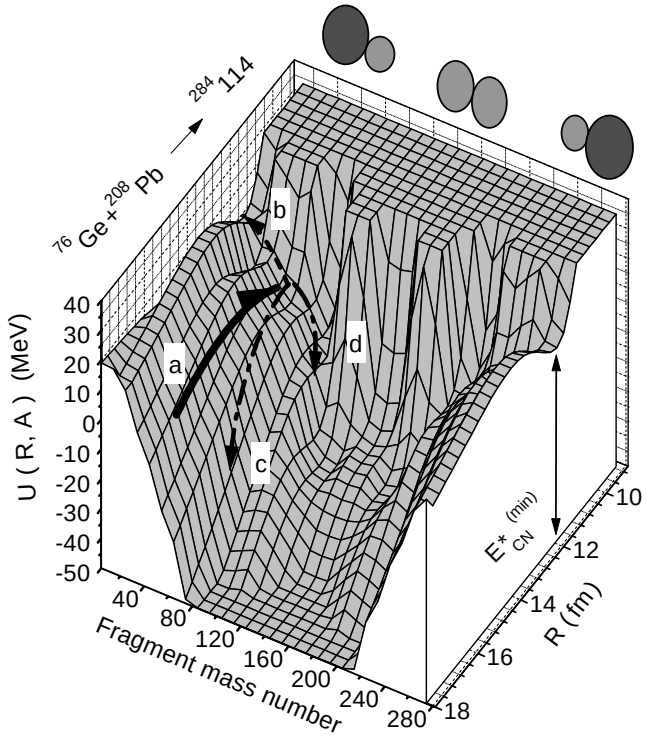

Fig. 4. Potential energy surface $U(A, R; \ell = 0)$ as function of the distance R between the centers of the nuclei and mass number A of a fragment. The arrows show directions of entrance (a), fusion (b), and quasi-fission (c,d) channels.

try axes. In our calculation the dependence of $V(R)$ from the orientation of the symmetry axes is included (fig. 2) by averaging over the orientation of the symmetry axis of the projectile α_1 with respect to the beam (fig. 3). The competition between complete fusion and quasi-fission of a dinuclear system formed after capture and its further evolution are described by $P_{\rm CN}$ using the method developed in [2]. This method is based on the assumption that the dinuclear system formed in the collision of two nuclei evolves to fusion by increasing its mass asymmetry. A path to fusion is determined by potential energy surface $U(A, Z; R)$ presented for the reaction ^{76}Ge+^{208}Pb in fig. 4. $U(A, Z; R)$ is calculated as a function of masses (charges) A_1, A_2 ($A_2 = A_{\rm tot} - A_1$) of fragments forming the dinuclear system and the distance R between their centers:

$$\begin{aligned} U(A, Z; R, \ell) &= U(A, Z, \ell, \beta_1, \alpha_1; \beta_2, \alpha_2) \\ &= B_1 + B_2 + V_0(Z, \ell, \beta_1, \alpha_1; \beta_2, \alpha_2; R) \\ &\quad -(B_0 + V_{\rm comp}(\ell)). \end{aligned} \tag{9}$$

Here, B_1, B_2 and B_0 are the binding energies of the nuclei in a dinuclear system and of the compound nucleus, respectively, which were obtained from [7] and from [8] particularly for the superheavy elements; β_i are the fragment deformation parameters and α_i are the orientations relative to the beam direction; $V_{\rm comp}(\ell)$ is the rotational energy of the compound nucleus. In this approach the mass asymmetry degree of freedom is the important dynamic variable to study the fusion process. The evolution of the system along the mass asymmetry degree of freedom is described by the driving potential $U(A, Z; R_{\rm m}, \ell)$. It is determined from the potential energy surface $U(A, Z; R, \ell)$ as a curve marking the bottom of the valley as a function of charge asymmetry (see fig. 4). The $R_{\rm m}$ is the position of this minimum (bottom of the pocket) on the R axis for a given mass asymmetry A_1. One can see from (9) and fig. 4 that sectional view of $U(A, Z, R; \ell = 0)$ at a given value of charge asymmetry Z is $V_0(R)$ moved on the Q-value between this charge asymmetry and complete fusion ($Q_{gg} = B_1 + B_2 - B_0$). The curve passes through the minimum of the nucleus-nucleus interaction potential for each value of mass asymmetry A_1 (on the (U, R)- plane). The driving potential $U(A, Z; R, \ell, \beta_1, \alpha_1; \beta_2, \alpha_2) \equiv U(A, Z; \ell)$ calculated in this way is presented in fig. 5. Note for the cases when there is no minimum of the nucleus-nucleus potential $V(R)$ (case of interaction of two massive symmetrical nuclei), $R_{\rm m}$ was got as a point where the nuclear part of the interaction potential $V_{\rm nucl}(R)$ has a minimum.

The ratios A_1/Z_1 and A_2/Z_2 for the fragments were determined by minimizing $U(A_1, Z_1; R)$ as a function of A_1 for each Z_1.

Therefore, a dinuclear system to be fused should overcome the intrinsic barrier ($B^*_{\rm fus}$) which is determined by the difference between the maximum of a driving potential and its value at the point corresponding to the initial charge asymmetry of the considered reaction (fig. 5). The smallest value of excitation energy of the compound nucleus ($E^{*({\rm min})}_{\rm CN}$) is determined by the top value of the driving potential (see fig. 5) which corresponds to the saddle point on the way to complete fusion (fig. 4). It should be noted that the shapes of the potential energy surface and driving potential depend on which mutual orientation of nuclei was used. The quasi-fission which is in competition with fusion is considered as a motion in the $V(R)$ nucleus-nucleus interaction potential (6). Thus, for quasi-fission, it is necessary to overcome a barrier of $V(R)$ on the R axis.

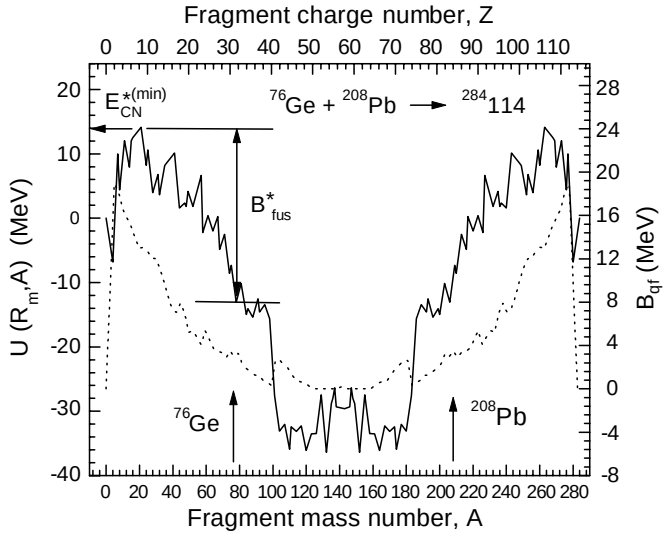

Fig. 5. The driving potential (solid curve, left axis) and quasi-fission barriers (dotted curve, right axis) for the superheavy nucleus $^{284}114$ as a function of mass (charge) number of a dinuclear system fragment. The vertical arrows indicate an initial charge asymmetry which corresponds to the reaction ^{76}Ge + ^{208}Pb. $E^{*(\min)}_{\rm CN}$ is the smallest possible value of the excitation energy of compound nucleus.

The competition between fusion and quasi-fission is taken into account by the factor $P_{\rm CN}(E,\ell)$ which is calculated using the following relation derived from the statistical model

$$P_{\rm CN} = \frac{\rho(E^*_{\rm DNS} - B^*_{\rm fus})}{\rho(E^*_{\rm DNS} - B^*_{\rm fus}) + \rho(E^*_{\rm DNS} - B_{\rm qf})}. \qquad (10)$$

Here $\rho(E^*_{\rm DNS} - B^*_{\rm K})$ is the level density

$$\rho(E^*_{\rm DNS} - B^*_K) = \frac{g(\varepsilon_{\rm F})K_{\rm rot}}{2\sqrt{g_1(\varepsilon_{\rm F})g_2(\varepsilon_{\rm F})}} \times \frac{\exp\left[2\pi\sqrt{g(\varepsilon_{\rm F})(E^*_{\rm DNS} - B^*_{\rm K})/6}\right]}{\left[\frac{3}{2}g(\varepsilon_{\rm F})(E^*_{\rm DNS} - B^*_{\rm K})\right]^{\frac{1}{4}}(E^*_{\rm DNS} - B^*_{\rm K})\sqrt{48}}. \qquad (11)$$

In eq. (10), $B_{\rm qf}$ is the barrier of the nucleus-nucleus interaction potential which needs to be overcome if the dinuclear system decays in two fragments, $E^*_{\rm DNS}$ is an excitation energy of the dinuclear system given by the difference between beam energy $E_{\rm c.m.}$ and the minimum of the nucleus-nucleus potential ($E^*_{\rm DNS} = E_{\rm c.m.} - V(R_{\rm m})$), $g_{1,2}(\varepsilon_{\rm F})$ are the single particle level densities of the fragments of the dinuclear system: $g_i = A_i\varepsilon_{\rm F}^{-1}(i = 1, 2)$ [9], $\varepsilon_{\rm F} = 37$ MeV and $g = g_1 + g_2$, $K_{\rm rot}$ is an enhancement factor at the level density which takes into account rotation of the dinuclear system

$$K_{\rm rot} = \frac{\sqrt{6(E^*_{\rm DNS} - B^*_{\rm K})/g(\varepsilon_{\rm F})}}{\pi} J_\perp, \qquad (12)$$

where

$$J_\perp = 2/5 m_0 r_0^2 A^{5/3}(1 + \beta_2/3) \qquad (13)$$

is the rigid body moment of inertia for rotation around the axis perpendicular to the line connecting the centers of fragments. In (13), $r_0 = 1.18$ fm, β_2 is the parameter of the fragment quadrupole deformation the value of which was obtained from [7] and [8]. For axially and mirror-symmetric nuclei, the $K_{\rm rot}$ enhancement factor is equal to $\sigma^2_\perp$, where $\sigma^2_\perp = (J_\perp T)/\hbar^2$ is the spin-dependent parameter and T is the effective nuclear temperature which was calculated by expression (A.14). The enhancement factor (12) of the level density describes an adiabatic limit in which intrinsic and rotational degrees of freedom are completely decoupled. This assumption ceases to be valid for higher excitation energies. Following [10,11], we account for the damping of the rotational enhancement multiplying the $K_{\rm rot}$ factor by

$$1 - Q_{\rm rot}\left(1 - \frac{1}{\hbar^2/J_\perp T}\right). \qquad (14)$$

This expression is tailored [11] to approach unity, essentially leaving the entire rotational contribution to the level densities intact, at temperatures T which are low compared with the Coriolis energy $E_{\rm cor}$, and tends to the inverse of the rotational enhancement factor $\hbar^2/J_\perp T$ at $T \gg E_{\rm cor}$, leading to the cancellation of the rotational enhancement. To this end, the $Q_{\rm rot}$ function is arbitrarily related to the Fermi-gas occupation probability of the single-particle levels at energy $E_{\rm cor}$

$$Q_{\rm rot} = \frac{2}{\exp(E_{\rm cor}/T) + 1}. \qquad (15)$$

In this expression the Coriolis energy may be approximated as [9,10]

$$E_{\rm cor}({\rm MeV}) \simeq \hbar\omega_0|\delta_{\rm osc}| = 41A^{-1/3}|\delta_{\rm osc}|, \qquad (16)$$

where $\hbar\omega_0$ is the mean oscillator frequency; $\delta_{\rm osc}$ is the potential deformation parameter. The ratio between this parameter and β_2 is determined by expression in [9]

$$\delta_{\rm osc} = 0.945\beta_2\left[1 - \frac{4}{3}\pi^2\left(\frac{a_0}{R_0}\right)^2\right] + 0.34\beta_2^2, \qquad (17)$$

where $a_0 = 0.54$ fm and $R_0 = r_0A^{1/3}$. In the second step of our estimations we calculate the evaporation cross-sections for the above-mentioned reactions from the fusion cross-sections. The advanced statistical model (ASM), described in detail in [6,11,12], allows us to take into account the dynamical aspect of the fission-evaporation competition at the compound nucleus evolution along the de-excitation cascade. The model accounts exactly for the angular momentum and parity coupling, allows for the neutron, proton, and α-particle multiple emission as well as for a fission channel and full γ-cascade in the residual nuclei. Particular attention is devoted to the determination of the level densities. These are calculated in the non-adiabatic approach allowing for rotational and vibrational enhancements. These collective effects are gradually removed above a certain energy. In the case of rotational

enhancement this energy is related to the Coriolis force which couples intrinsic and collective motions. Our level densities acquire a dynamic aspect through the dependence of the Coriolis force and of the rotational enhancement on the nuclear shape, which is, in turn, obtained from the classical model of the rotating liquid drop. Intrinsic level densities are calculated using the Ignatyuk approach [13] which takes into account shell structure effects and pairing correlation. Use of the correct level densities is of fundamental importance for the present analysis as they determine the phase space available for each channel, a very essence that governs any statistical decay. In the case of the evaporation residue production one should also carefully consider the low energy level densities since this is the energy interval in which most of the evaporation residues are formed. That is why we use the super-fluid model of the nucleus [14] in our calculations with the standard value of pairing correction $\Delta = 12/\sqrt{A}$. The yrast lines are automatically included in our calculations by the requirement that the total excitation energy should be higher than the rotational one, otherwise the level density is set to zero.

As far as the fission barriers are concerned, we use the rotating droplet model predictions (angular momentum dependent) as parameterized by Sierk [15] and allow for angular momentum and temperature fade-out of the shell corrections [6]. This is expressed by the formula for the actual fission barrier used in our calculations:

$$B_{\rm fis}(J,T) = c\ B^{m}_{\rm fis}(J) - h(T)\ q(J)\ \delta W, \qquad (18)$$

with

$$h(T) = \begin{cases} 1\,, & T \leq 1.65\ \text{MeV}\,, \\ k\exp\left(-mT\right), & T > 1.65\ \text{MeV}, \end{cases}$$

and

$$q(J) = \{1 + \exp[(J - J_{1/2})/\Delta J]\}^{-1},$$

where $B^{\rm m}_{\rm fis}(J)$ is the parameterized macroscopic fission barrier [15] depending on angular momentum J, $\delta W = \delta W_{\rm sad} - \delta W_{\rm gs} \simeq -\delta W_{\rm gs}$ is the microscopic (shell) correction to the fission barrier taken from the tables [8] and the constants for the macroscopic fission barrier scaling, temperature and angular momentum dependencies of the microscopic correction are chosen to be as follows: $c = 1.0$, $k = 5.809$, $m = 1.066\ \text{MeV}^{-1}$, $\Delta J = 3\hbar$; for nuclei with $Z > 102$ we use $J_{1/2} = 20\hbar$. This procedure let the shell corrections become dynamical quantities, too.

Dissipation effects, which delay fission, are treated according to [16,17]. These include Kramers' stationary limit [18] and an exponential factor applied to Kramers' fission width to account for the transient time, after which the statistical regime is reached. The systematic obtained by Bhattacharya *et al.* [19] gives the possibility of taking into account the incident energy per nucleon ϵ and compound nucleus mass $A_{\rm CN}$ dependencies of the reduced dissipation coefficient $\beta_{\rm dis}$. $\beta_{\rm dis}$ is the ratio between the friction coefficient γ describing the coupling to the fission degree of freedom and the reduced mass m of the system. This ratio characterizes the dissipative and diffusive motion. In the calculations we used the simple form

$$\beta_{\rm dis}(\epsilon, A_{\rm CN}) = a\epsilon + bA^{3}_{\rm CN}, \qquad (19)$$

where $a = 0.18$ and $b = 0.357 \times 10^{-6}$ [19]. For the investigated reactions the $\beta_{\rm dis}$ values range from 6 to $7 \times 10^{21}\ \text{s}^{-1}$.

In the present ASM calculations the target-projectile fusion cross-section was determined by formula (2).

3 Results

The effect of the entrance channel can be studied by comparing the calculated evaporation residue cross-sections with experimental ones. The dinuclear concept allows us to consider the dinuclear system formation sequence, its evolution to complete fusion or to competitive quasi-fission stages. These stages are characterized by the capture cross-section (which is the probability of the dinuclear system formation), the intrinsic fusion barrier $B^{*}_{\rm fus}$, and the excitation energy $E^{*}_{\rm DNS}$ of the dinuclear system. According to the scenario of the DNS-concept, if the maximum value of $E^{*}_{\rm DNS}$ is lower than $B^{*}_{\rm fus}$, then the dinuclear system cannot be transformed into a compound nucleus and for all values of beam energy, the heavy ion collisions end in deep inelastic (damped) collisions or quasi-fission processes. The reason is that the capture and fusion processes have energy windows determined by the particular characteristics of the entrance channel: the mass and charge of the colliding nuclei, their shape and shell structure, the beam energy and orbital angular momentum, because the potential energy surface is a function of the quantities defined above. The capture is determined by peculiarities of the nucleus-nucleus potential which depends on the nuclear shape and orbital angular momentum. The quasi-fission barrier $B_{\rm qf}$ is calculated as a depth of the potential well in $V(R(t))$ which includes the change due to nucleon exchange and particle-hole excitations in nuclei. The ratio between the intrinsic fusion barrier $B^{*}_{\rm fus}$ and the quasi-fission barrier $B_{\rm qf}$ plays a decisive role for the formation of the compound nucleus. As seen from Table 1 the dependence of these quantities on the charge (and mass) of the compound nucleus being formed at the indicated beam energy is strong: the intrinsic fusion barrier $B^{*}_{\rm fus}$ increases with atomic number of the projectile when the same target-nucleus is used. The ratio $B_{\rm qf}/B^{*}_{\rm fus}$ decreases gradually from 0.53 which is obtained for the reaction ^{50}Ti $+^{208}$Pb to 0.07 for the reaction ^{86}Kr $+^{208}$Pb. The maximum value of the possible excitation energy $E^{*(\rm max)}_{\rm DNS}$ of the dinuclear system is determined by the largest initial beam energy leading to formation of the dinuclear system and the minimum of the well of the nucleus-nucleus potential $V(R)$. The kinetic energy of the collision is transformed into excitation energy of the nuclei due to the interaction of the motion of nucleons inside the nuclei and the relative motion of the nuclei. This excitation energy value decreases when the lifetime of the dinuclear system becomes shorter. This time is determined by the beam energy and the depth of the potential well which decreases when the total charge

Table 1. The calculated maximum value of the beam energy $E_{\rm lab}^{(\rm max)}$ leading to the formation of a dinuclear system, and the corresponding excitation energy of the compound nucleus (CN) $E_{\rm CN}^{*(\rm max)}$ and the dinuclear system $E_{\rm DNS}^{*(\rm max)}$ for the considered reactions. The intrinsic fusion barrier $B_{\rm fus}^{*}$ and quasi-fission barrier $B_{\rm qf}$ determine the competition between complete fusion and quasi-fission in the dinuclear system concept. The range $E_{\rm DNS}^{*(\rm max)} - B_{\rm fus}^{*} = \Delta E_{\rm DNS}^{*}$ characterizes the width of the energy window for fusion at the given entrance channel.

Reaction	CN	$E_{\rm lab}^{(\rm max)}$ (MeV)	$E_{\rm CN}^{*(\rm max)}$ (MeV)	$E_{\rm DNS}^{*(\rm max)}$ (MeV)	$B_{\rm fus}^{*}$ (MeV)	$B_{\rm qf}$ (MeV)	$B_{\rm qf}/B_{\rm fus}^{*}$	$\Delta E_{\rm DNS}^{*}$ (MeV)
^{50}Ti + ^{208}Pb	^{258}104	286.5	61.50	45.50	13.55	7.24	0.53	32.0
^{58}Fe + ^{208}Pb	^{266}108	297.0	28.38	30.20	16.61	4.94	0.30	13.6
^{64}Ni + ^{208}Pb	^{272}110	330.0	26.10	26.50	17.61	3.61	0.20	8.9
^{64}Ni + ^{209}Bi	^{273}111	328.3	23.56	23.57	15.30	2.78	0.18	8.3
^{70}Zn + ^{208}Pb	^{278}112	347.5	15.82	22.00	20.52	3.42	0.17	1.5
^{70}Zn + ^{209}Bi	^{279}113	350.0	14.45	22.18	19.30	3.27	0.17	2.8
^{76}Ge + ^{208}Pb	^{284}114	387.5	21.25	26.35	23.12	3.23	0.16	3.2
^{86}Kr + ^{208}Pb	^{294}118	450.0	15.77	21.05	20.42	1.36	0.07	0.6

number of the system increases or when the mass asymmetry of colliding nuclei decreases. The calculations show that capture of nuclei is possible at higher energies leading to the formation of the rotating dinuclear system when there is a potential well of the nucleus-nucleus interaction. But the increase of the orbital angular momentum leads to an increase of the intrinsic fusion barrier $B_{\rm fus}^{*}$ and a decrease of the quasi-fission barrier due to rotational energy. As a result, the fusion cross-section decreases drastically and the amalgamation of nuclei becomes more difficult.

The measured and calculated excitation functions for the production of the superheavy elements from rutherfordium ($Z = 104$) to element 112 by the cold fusion reactions ^{50}Ti +^{208}Pb, ^{50}Fe +^{208}Pb, ^{64}Ni +^{208}Pb, ^{64}Ni +^{209}Bi and ^{70}Zn +^{208}Pb are presented in figs. 6-10. In these figures and in figs. 11 and 12, the thicker solid curve shows the fission barrier ($B_{\rm fis}(J,T)$) of the compound nucleus formed in the considered reactions. Its value is labeled on the right axis. $B_{\rm fis}(J,T)$ was calculated by eq. (18). The dashed line shows the fusion cross-section calculated by eq. (2) and the dotted line shows the calculated quasi-fission cross-section that is obtained as a difference between the capture cross-section calculated by eq.(3) and the fusion cross-section. The values are labeled on the left axis. The top axis shows the excitation energy E^{*} of the compound nucleus. Its value is connected with the beam energy $E_{\rm lab}$ presented on the bottom axis:

$$E^{*} = E_{\rm lab}\frac{A_{\rm T}}{A_{\rm P}+A_{\rm T}} + Q_{gg}$$

where Q_{gg} is the reaction Q-value.

In fig. 6, the symbols with the error bars show the measured excitation functions of the evaporation residue production for the reaction ^{50}Ti +^{208}Pb; in the upper panel, diamonds and thin solid curve mark the total measured and calculated evaporation residue cross-section, respectively. In the bottom panel, the measured 1n-, 2n-, and 3n- excitation functions are presented by the solid circles, open triangles, and solid squares, respectively. The calculated excitation functions of the 1n-, 2n-, 3n-evapora- tion channels are shown by the dot-dashed, dot-dot-dashed and short dashed curves. The calculation shows a maximum value of the excitation function for an energy window which is determined by the entrance channel of the reaction. The evaporation residue cross-section $\sigma_{\rm er}$ depends on the survival probability $W_{\rm sur}(E,\ell)$ during the de-excitation cascade at the bombarding energy E and orbital angular momentum ℓ.

In the synthesis of elements $Z = 110, 111$ and 112 only the 1n-evaporation channel was observed, in the case of hassium ($Z = 108$) also the 2n channel. In figs, 7-10, the measured excitation functions are shown by solid circles with error bars. The calculated excitation functions of 1n- and 2n-evaporation channel are presented by the dot-dashed and dot-dot-dashed curves, respectively.

The comparison between the experimental results and calculations for the reactions ^{56}Fe + ^{208}Pb, ^{64}Ni+^{208}Pb, ^{64}Ni+^{209}Bi, and ^{70}Zn+^{208}Pb is presented in figs. 7-10. The use of a microscopic approach including shell effects for fusion and of the advanced statistical model for the de-excitation cascade in our calculations allows us to obtain excitation functions in good agreement with the measured evaporation residues.

In Table 1 we compare the values for the intrinsic fusion barrier $B_{\rm fus}^{*}$ and the maximum excitation energy of the dinuclear system $E_{\rm DNS}^{*(\rm max)}$ for the investigated reactions. Moreover, the difference $E_{\rm DNS}^{*(\rm max)} - B_{\rm fus}^{*}$ characterizes the energy window $\Delta E_{\rm DNS}^{*}$ for fusion at the given entrance channel. One can see from Table 1 that for the reactions leading to the more massive compound nuclei the $\Delta E_{\rm DNS}^{*}$ interval decreases, and consequently the beam energy window that contributes to the fusion cross-section decreases.

The minimum value of the calculated excitation energy ($E_{\rm CN}^{*(\rm min)}$) is determined by the maximum value of the driving potential which is at the charge (mass) numbers between $Z = 0$ and $Z = Z_{\rm P}$ (for the case $Z_{\rm P} < Z_{\rm T}$, see fig. 5). It corresponds to the value of the potential energy surface at the saddle point on the way to

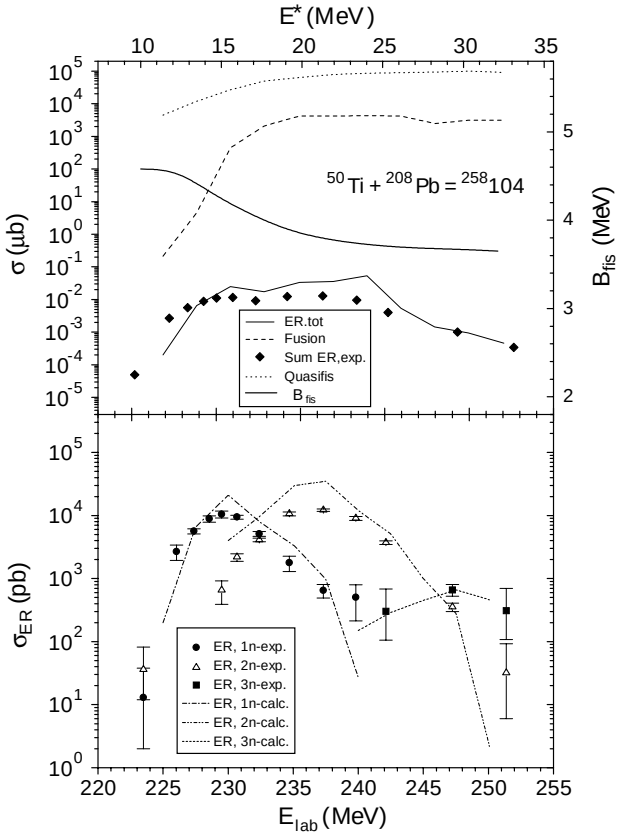

Fig. 6. Top panel: the calculated quasi-fission (dotted curve), fusion (dashed curve), total evaporation residue (thin solid curve) excitation functions and the measured total evaporation residue excitation function (diamonds) as a function of excitation energy of the compound nucleus for the reaction ^{50}Ti + ^{208}Pb (left ordinate axis). The thick solid curve shows the fission barrier for the compound nucleus ^{258}Rf (right ordinate axis). Bottom panel: measured (symbols) excitation function for production of rutherfordium by the same reaction as function of beam energy $E_{\rm lab}$ (energy in the middle of the target, scale at the bottom axis) and excitation energy E^* (scale at the top axis): solid circles, open triangles, and solid squares are for 1n-, 2n-, 3n-evaporation channels, respectively. The calculated results (curves) for the corresponding quantities: dot-dashed, dot-dot-dashed and short-dashed curves are for 1n-, 2n-, 3n-evaporation channels, respectively.

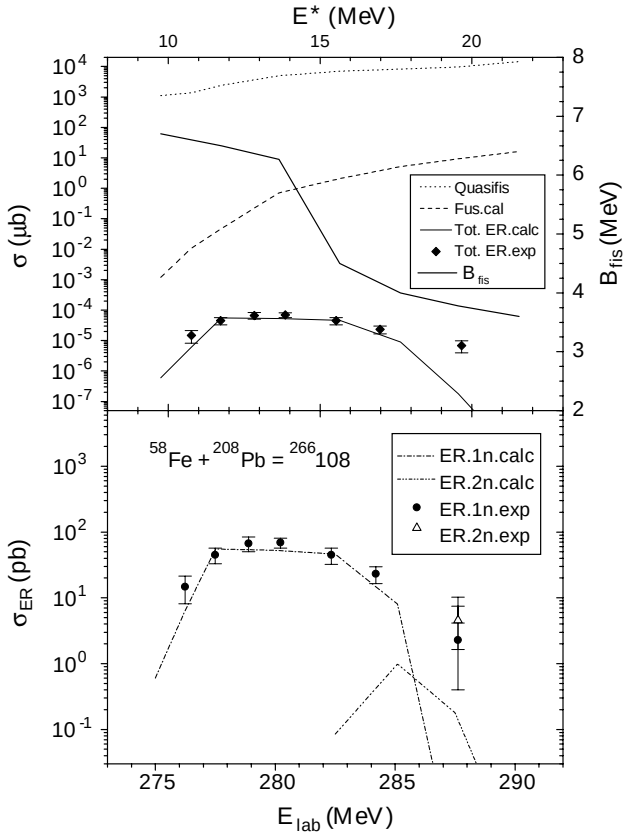

Fig. 7. Same as fig. 6, but for the reaction ^{58}Fe + ^{208}Pb.

fusion. In Table 2, the calculated values of $E^{*(\rm min)}_{\rm CN}$ are compared with the minimum values of excitation energy $E^{*(\rm min)}_{\rm exp}$ at which the evaporation residues were measured in the experiments in GSI for synthesis of superheavy elements $Z = 104, 108, 110, 111$ and 112 and at Berkeley for $Z = 118$ [20]. For all investigated reactions, the experimental point of the residue nucleus formation after one-neutron emission from the excited compound nucleus corresponding to the smallest value of the excitation energy $E^*_{\rm exp}$ is in agreement with the calculated minimum excitation energy $E^{*(\rm min)}_{\rm CN}$, or it is a little higher ($E^*_{\rm exp} = 12.7$ MeV in comparison with $E^{*(\rm min)}_{\rm CN} = 10.9$ MeV) for the compound nucleus ^{273}111. This is because at $E^*_{\rm CN}$ of about

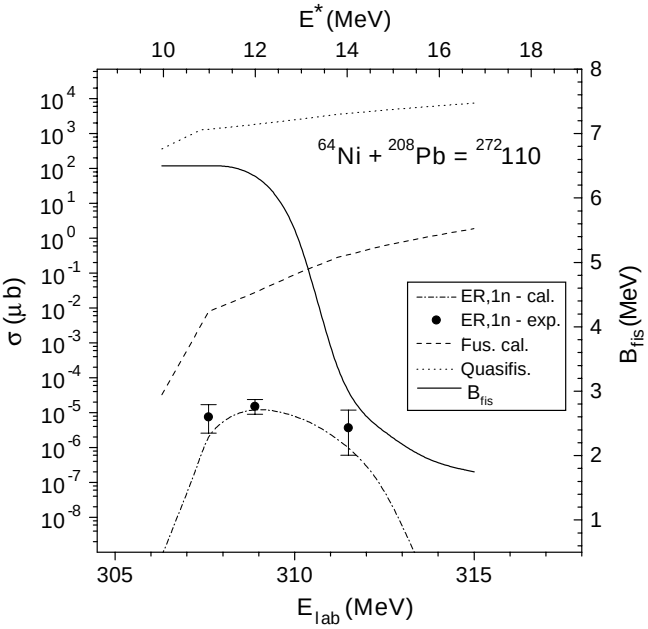

Fig. 8. The calculated quasi-fission (dotted curve), fusion (dashed curve) and 1n-evaporation residue excitation functions (left axis) for the reaction ^{64}Ni+^{208}Pb. The solid curve shows the fission barrier for the compound nucleus ^{272}110 (right ordinate axis). The measured and calculated 1n-excitation functions are shown by solid circles and dot-dashed curve, respectively.

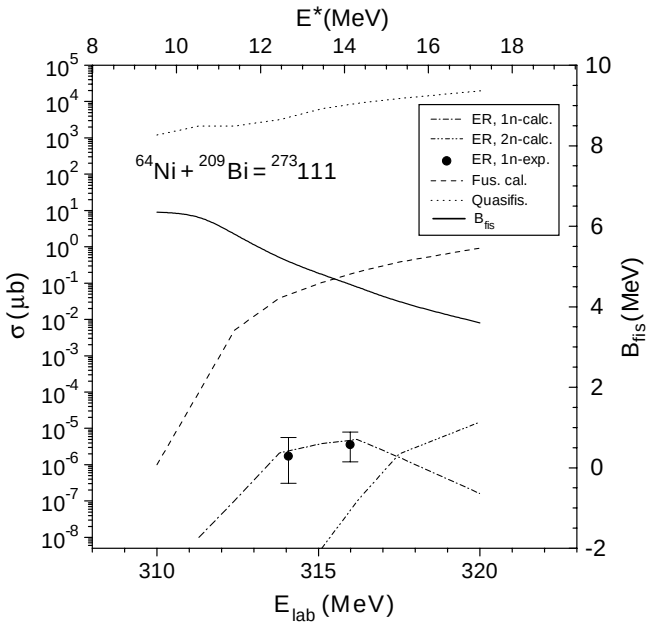

Fig. 9. Same as fig. 8, but for the reaction ^{64}Ni+^{209}Bi.

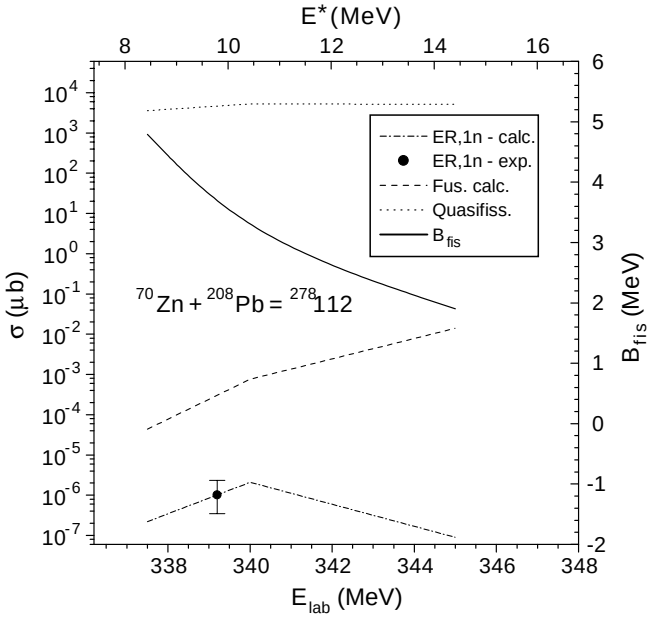

Fig. 10. Same as fig. 8, but for the reaction ^{70}Zn+^{208}Pb.

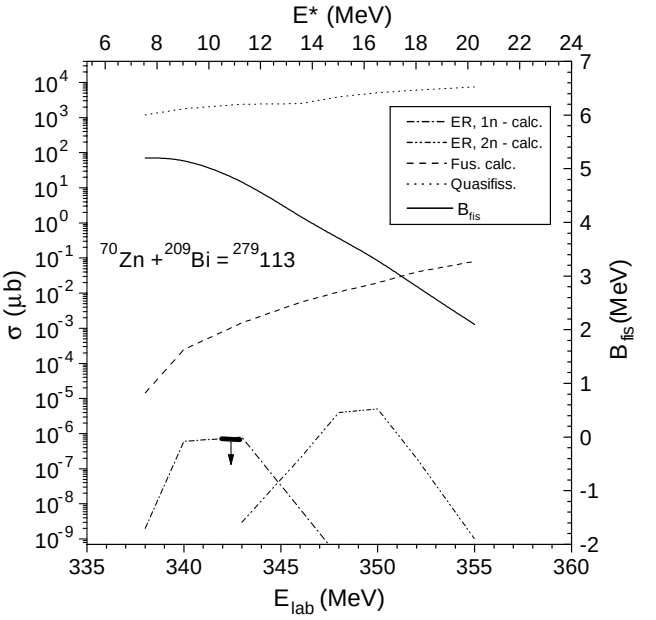

Fig. 11. Same as fig. 8, but for the reaction ^{70}Zn+^{209}Bi. The thick horizontal line with the arrow is the upper limit for the 1n-evaporation channel obtained in the experiment at GSI.

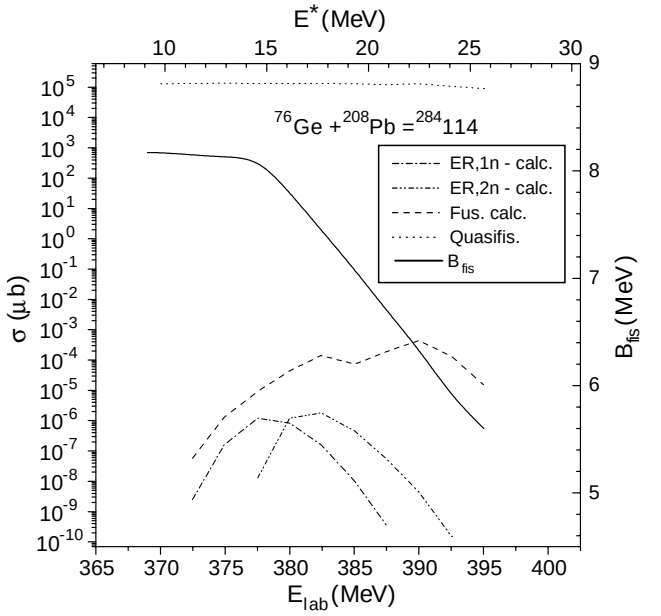

Fig. 12. Same as fig. 8, but for the reaction ^{76}Ge+^{208}Pb.

10.9 MeV the fusion cross-section is lower than 10^{-10} mb, and a residue cross-section is lower than 10^{-13} mb. It is practically impossible to receive experimental data below excitation energies of $E^*_{\rm CN} = 10.9$ MeV. Our calculations predict that only at excitation energies between 12 and 14 MeV the cross-sections reach values above 1 pb. The evaporation residue measurements by *cold fusion reactions* are limited at lower excitation energies by the intrinsic fusion barrier $B^*_{\rm fus}$ which leads to fusion cross-sections of the order of 10^{-5} mb at values of $E^*_{\rm CN}$ of about 10 MeV. At excitation energies higher than about 20 MeV the synthesis of evaporation residues is limited by increasing fission probability of the compound nucleus (in competition with light particle emission) due to the strong decrease of the fission barrier.

The evaporation residue excitation functions for the synthesis of the superheavy elements $Z = 113$ and $Z = 114$ by the reactions ^{70}Zn + ^{209}Bi and ^{76}Ge + ^{208}Pb, respectively, were estimated using the same value for the r_0 parameter. The results are presented in figs. 11 and 12. In these figures, the fusion cross-section is presented by the dashed curve, the excitation functions of the 1n-

Table 2. The comparison between the calculated minimum value of excitation energy for the compound nucleus (CN) $E^{*(\min)}_{\rm CN}$ and the measured one $E^{*(\min)}_{\rm exp}$.

CN	$E^{*(\min)}_{\rm CN}$ (MeV)	$E^{*(\min)}_{\rm exp}$ (MeV)
$^{258}104$	10.9	10.2
$^{266}108$	10.3	10.8
$^{272}110$	10.5	11.1
$^{273}111$	10.9	12.7
$^{278}112$	8.9	10.0
$^{279}113$	16.2	–
$^{284}114$	14.1	–
$^{294}118$	18.0	13.3

and 2n-evaporation channel are shown by dot-dashed and dot-dot-dashed curves, respectively. The maximum of the excitation function for the 2n-evaporation channel is larger than for the 1n-evaporation channel. In the case of the reaction ^{70}Zn + ^{209}Bi the calculated evaporation residue cross-section after 2-neutron emission is some picobarns at $E^* \simeq 16$ MeV or $E_{\rm lab} \simeq 350$ MeV. The upper limit for the 1-n evaporation channel obtained in the experiment at GSI in March-April 1998 was 0.6 pb at $E^* = 10.7$ MeV.

In the framework of the used model based on the DNS concept, we also performed calculation for the ^{86}Kr + ^{208}Pb reaction leading to the compound nucleus $^{294}118$. We obtained information on the entrance channel dynamics (see Tables 1 and 2). We also estimated the upper limit of the cross-section for the superheavy nucleus $^{293}118$ to be about 4.6×10^{-3} pb. This value is much lower than the one measured by the Berkeley group [20].

4 Conclusion

The combined dynamical and statistical model based on the dinuclear system approach allowed us to estimate excitation functions of quasi-fission, fusion, and formation of evaporation residues in *cold* fusion reactions with massive nuclei. The capture stage was calculated using the dynamical model and for calculation of the fusion stage a statistical approach was used. The obtained optimal beam energy or excitation energy of the compound nucleus is in good agreement with the experimental data. The fusion excitation functions calculated in this way were used to estimate the surviving probability of the formed compound nucleus relative to fission in the frame of the advanced statistical model for the de-excitation cascade. The excitation functions obtained in this paper are in good agreement with the ones measured in the GSI experiments. The observed decrease of the width of excitation functions seems to be connected with the decreasing ratio between quasi-fission barrier $B_{\rm qf}$ and intrinsic barrier $B^*_{\rm fus}$ which means that the potential well becomes smaller for the systems formed from more massive fragments. Moreover, the beam energy window that contributes to the capture (and then to the fusion production) is related to the energy range $\Delta E^*_{\rm DNS}$. In addition, the evaporation residue measurements for *cold fusion reactions* are limited to lower excitation energies by the height of the saddle point of the potential energy surface $U(A, Z; R, \ell)$ on the way to fusion ($E^{*(\min)}_{\rm CN}$), and for higher excitation energies they are limited by the fission process due to the strong decrease of the fission barrier.

The effect of the entrance channel was studied by analyzing the quantities in detail which were used in the calculation of the fusion cross-section. These are the capture cross-section (which is the formation probability of the dinuclear system in competition with quasi-fission), the intrinsic fusion barrier $B^*_{\rm fus}$, the quasi-fission barrier $B_{\rm qf}$, and the excitation energy $E^*_{\rm DNS}$ of the dinuclear system. According to the scenario of the DNS-concept, if the maximum value of $E^*_{\rm DNS}$ is lower than $B^*_{\rm fus}$ the dinuclear system cannot be transformed into a compound nucleus. The entrance channel dynamics for the ^{86}Kr + ^{208}Pb reaction is close to such a critical condition. In the framework of the DNS model, we estimate the value of 0.6 MeV (see Table 1) for the $E^*_{\rm DNS}$ energy window that can lead to the fusion of the dinuclear system, and then to the formation of the superheavy element with Z=118. The difference ($E^{*(\max)}_{\rm DNS} - B^*_{\rm fus}$) characterizes the energy window for fusion at a given entrance channel. It means that only those theoretical approaches which include the peculiarities of projectile and target nuclei, as well as dynamics of the reaction mechanisms, are able to predict the height, width and position of the energy window favorable for the synthesis of superheavy elements. We found that, for the reaction ^{70}Zn + ^{209}Bi, the maximum of the excitation function for the 2n-evaporation channel is larger than for the 1n-evaporation channel: the calculated cross-section of the evaporation residue is some picobarns at $E^* \simeq 16$ MeV or $E_{\rm lab} \simeq 350$ MeV. The measured upper limit in the experiment at GSI in March-April 1998 was 0.6 pb at $E^* = 10.7$ MeV. It is anticipated that the increase of the beam energy to get $E^* \simeq 16$ MeV would be favorable to observe events of the synthesis of element $Z = 113$. The estimated upper limit of the cross-section for the superheavy nucleus $^{293}118$ to be about 4.6×10^{-3} pb. This value is much lower than the one measured by the Berkeley group [20].

We are grateful to Prof. V.V. Volkov for helpful discussion. One of the authors (A.K.N.) thanks the Heisenberg-Landau Program for support while staying at the Gesellschaft für Schwerionenforschung, Russian Fund of Basic Research (Grant No.97-02-16030) and agricultural LTD "Davron" by K. Nasirov (Andijan, Uzbekistan) for financial support. Authors A.I.M and A.K.N. are grateful to the Uzbekistan State Scientific-Technical Committee (Grant No. 4/98) for partial support. A.K.N. would like to express his gratitude for the warm hospitality during his stay at GSI.

Appendix A.

The nucleus-nucleus potential is calculated as follows:

$$V_0(\mathbf{R}) = V_{\rm C}(\mathbf{R}) + V_{\rm nucl}(\mathbf{R}) + V_{\rm rot}(\mathbf{R}), \tag{A.1}$$

where $V_C(\mathbf{R})$, $V_{\rm nucl}(\mathbf{R})$, and $V_{\rm rot}(\mathbf{R})$ are the Coulomb, nuclear, and rotational potentials, respectively. The nuclear shape is important in the calculation of the Coulomb and the nuclear interactions between colliding nuclei. Thus, the Coulomb interaction of deformed nuclei (with a quadrupole deformation) can be calculated according to the following expression taken from [21]:

$$\begin{aligned} V_C(R) = {} & \frac{Z_1 Z_2}{R} e^2 \\ & + \frac{Z_1 Z_2}{R^3} e^2 \left\{ \left(\frac{9}{20\pi} \right)^{1/2} \sum_{i=1}^{2} R_{0i}^2 \beta_2^{(i)} \mathcal{P}_2(\cos\alpha_i') \right. \\ & \left. + \frac{3}{7\pi} \sum_{i=1}^{2} R_{0i}^2 \left[\beta_2^{(i)} \mathcal{P}_2(\cos\alpha_i') \right]^2 \right\}, \end{aligned} \tag{A.2}$$

where $\alpha_1' = \alpha_1 + \Theta$, $\alpha_2' = \pi - (\alpha_2 + \Theta)$, $\sin\Theta = |\mathbf{L}|/(\mu \dot{R} R)$; Z_i, $\beta_2^{(i)}$, and α_i' are (for each fragment) the atomic number, the quadrupole deformation parameter, and the angle (see fig. 3) between the line connecting the centers of mass of the nuclei and the symmetry axis of the fragment $i (i = 1, 2)$, respectively. Here, $R_{0i} = r_0 A_i^{1/3}, r_0 = 1.18$ fm and $\mathcal{P}_2(\cos\alpha_i')$ is the second term of the second type of Legendre polynomial.

The nuclear part of the nucleus-nucleus potential is calculated using the folding procedure between the effective nucleon-nucleon forces $f_{\rm eff}[\rho(x)]$ suggested by Migdal [22] and the nucleon density of the projectile- and the target-nucleus:

$$V_{\rm nucl}(R) = \int \rho_1^{(0)}(\mathbf{r} - \mathbf{R}_1) f_{\rm eff}[\rho] \rho_2^{(0)}(\mathbf{r} - \mathbf{R}_2) {\rm d}^3\mathbf{r}\,, \tag{A.3}$$

$$f_{\rm eff}[\rho] = 300 \left(f_{\rm in} + (f_{\rm ex} - f_{\rm in}) \frac{\rho(0) - \rho(r)}{\rho(0)} \right). \tag{A.4}$$

Here $f_{\rm in} = 0.09$, $f_{\rm ex} = -2.59$ are the constants of the effective nucleon-nucleon interaction; $\rho = \rho_1^{(0)} + \rho_2^{(0)}$; $\mathbf{R}_i$ $(i = 1, 2)$ is the position of the center of mass of the fragment i. The nucleon densities are assumed to have a Fermi distribution:

$$\begin{aligned} \rho_i^{(0)}(\mathbf{r} - \mathbf{R}_i) &= \rho_i^{(0)}(\mathbf{r}, \mathbf{R}_i(t), \beta_2^{(i)}, \beta_3^{(i)}) \\ &= \left\{ 1 + \exp\left[\frac{|\mathbf{r} - \mathbf{R}_i(t)| - \tilde{R}_i(\beta_2^{(i)}, \beta_3^{(i)})}{a_0} \right] \right\}^{-1}, \end{aligned} \tag{A.5}$$

$$\tilde{R}_i(\beta_2^{(i)}, \beta_3^{(i)}) = R_{0i}(1 + \beta_2^{(i)} Y_{20}(\alpha_i) + \beta_3^{(i)} Y_{30}(\alpha_i)), \tag{A.6}$$

where $a_0 = 0.54$ fm. The shape of the nuclei of the dinuclear system changes with the evolution of the mass asymmetry degrees of freedom: $\beta_2 = \beta_2(Z, A)$ and $\beta_3 = \beta_3(Z, A)$. In order to calculate the potential energy surface as a function of the charge number, we use the values of $\beta_2^{(2^+)}$ from the data in [23] and the values of $\beta_3^{(3^-)}$ from the data in [24].

Expressions for the friction coefficients

$$\gamma_R(R(t)) = \sum_{i,i'} \left| \frac{\partial V_{ii'}(R(t))}{\partial R} \right|^2 B_{ii'}^{(1)}(t), \tag{A.7}$$

$$\gamma_\theta(R(t)) = \frac{1}{R^2} \sum_{i,i'} \left| \frac{\partial V_{ii'}(R(t))}{\partial \theta} \right|^2 B_{ii'}^{(1)}(t), \tag{A.8}$$

and the dynamic contribution to the nucleus-nucleus potential

$$\delta V(R(t)) = \sum_{i,i'} \left| \frac{\partial V_{ii'}(R(t))}{\partial R} \right|^2 B_{ii'}^{(0)}(t), \tag{A.9}$$

were obtained in [5] by estimating the evolution of the coupling term between relative motion of nuclei and nucleon motion inside nuclei; $B_{ii'}^{(0)}(t)$ is given by eq. (A.11).

The dynamic correction of the reduced mass $\delta\mu(R(t))$ is calculated using the expression

$$\delta\mu(R(t)) = \sum_{i,i'} \left| \frac{\partial V_{ii'}(R(t))}{\partial R} \right|^2 B_{ii'}^{(2)}(t), \tag{A.10}$$

where $B_{ii'}^{(2)}(t)$ is given by eq. (A.3).

$$\begin{aligned} B_{ik}^{(n)}(t) = {} & \frac{2}{\hbar} \int_0^t {\rm d}t' (t - t')^n \exp\left(\frac{t' - t}{\tau_{ik}} \right) \\ & \times \sin\left[\omega_{ik}\left(\mathbf{R}(t')\right)(t - t') \right] [\tilde{n}_k(t') - \tilde{n}_i(t')], \end{aligned} \tag{A.11}$$

$$\hbar\omega_{ik} = \varepsilon_i + \Lambda_{ii} - \varepsilon_k - \Lambda_{kk}\,. \tag{A.12}$$

Here $\tilde{n}_i$ is a diagonal matrix element of the density matrix which is calculated according to the model presented elsewhere [5,25]; $\tau_{ik} = \tau_i \tau_k/(\tau_i + \tau_k)$; τ_i is the life time of the quasiparticle excitations in the single-particle state i of nucleus. It determines the damping of single-particle motion. The value of τ_i is calculated using the results of the theory of quantum liquids [26] and the effective nucleon-nucleon forces from [22]:

$$\begin{aligned} \frac{1}{\tau_i^{(\alpha)}} = {} & \frac{\sqrt{2}\pi}{32\hbar\varepsilon_{F_{\rm K}}^{(\alpha)}} \left[(f_{\rm K} - g)^2 + \frac{1}{2}(f_{\rm K} + g)^2 \right] \\ & \times \left[\left(\pi T_{\rm K} \right)^2 + \left(\tilde{\varepsilon}_i - \lambda_{\rm K}^{(\alpha)} \right)^2 \right] \\ & \times \left[1 + \exp\left(\frac{\lambda_{\rm K}^{(\alpha)} - \tilde{\varepsilon}_i}{T_{\rm K}} \right) \right]^{-1}, \end{aligned} \tag{A.13}$$

where

$$T_{\rm K}(t) = 3.46 \sqrt{\frac{E_{\rm K}^*(t)}{\langle A_{\rm K}(t) \rangle}} \tag{A.14}$$

is the effective temperature determined by the amount of intrinsic excitation energy $E_{\rm K}^* = E_{\rm K}^{*(Z)} + E_{\rm K}^{*(N)}$ and by the mass number $\langle A_{\rm K}(t) \rangle$ (with $\langle A_{\rm K}(t) \rangle = \langle Z_{\rm K}(t) \rangle + \langle N_{\rm K}(t) \rangle$).

In addition, $\lambda_{\rm K}^{(\alpha)}(t)$ and $E_{\rm K}^{*(\alpha)}(t)$ are the chemical potential and intrinsic excitation energies for the proton ($\alpha = Z$) and neutron ($\alpha = N$) subsystems of the nucleus K (K = 1(projectile), 2(target)), respectively. Furthermore, the finite size of the nuclei and the difference between the numbers of neutrons and protons makes it necessary to use the following expressions for the Fermi energies [22]:

$$\varepsilon_{F_{\rm K}}^{(Z)} = \varepsilon_{\rm F}\left[1 - \frac{2}{3}\big(1+2f'_{\rm K}\big)\frac{\langle N_{\rm K}\rangle - \langle Z_{\rm K}\rangle}{\langle A_{\rm K}\rangle}\right],$$
$$\varepsilon_{F_{\rm K}}^{(N)} = \varepsilon_{\rm F}\left[1 + \frac{2}{3}\big(1+2f'_{\rm K}\big)\frac{\langle N_{\rm K}\rangle - \langle Z_{\rm K}\rangle}{\langle A_{\rm K}\rangle}\right], \qquad \text{(A.15)}$$

where $\varepsilon_{\rm F}$=37 MeV,

$$f_{\rm K} = f_{\rm in} - \frac{2}{\langle A_{\rm K}\rangle^{1/3}}(f_{\rm in} - f_{\rm ex}),$$
$$f'_{\rm K} = f'_{\rm in} - \frac{2}{\langle A_{\rm K}\rangle^{1/3}}(f'_{\rm in} - f'_{\rm ex}) \qquad \text{(A.16)}$$

and $f_{\rm in} = 0.09$, $f'_{\rm in} = 0.42$, $f_{\rm ex} = -2.59$, $f'_{\rm ex} = 0.54$, $g = 0.7$ are the constants of the effective nucleon-nucleon interaction.

Finally, the rotational potential is:

$$V_{\rm rot}(R) = \hbar^2 \frac{l(l+1)}{2\mu R^2}. \qquad \text{(A.17)}$$

Appendix B.

The angles between the symmetry axis of the projectile- and target-nucleus and the beam direction are α_1 and α_2, respectively, (fig. 3). The spherical coordinate system O with the vector $\mathbf{r}$, angles θ and ϕ is placed at the mass center of the target-nucleus and the Oz axis is directed opposite to the beam. In this coordinate system, the direction of the vector $\mathbf{R}$ connecting the mass centers of the interacting nuclei has angles Θ and Φ. The coordinate system is chosen so that the planes, in which the symmetry axes of nuclei are located, cross the Oz line and form an angle Φ. For head-on collisions is $\Theta = 0$ and $\Phi = \phi$.

The nucleon distribution functions of interacting nuclei in the integrand (A.3) can be expressed using these variables in the same coordinate system O.

In the O system the symmetry axis of the target-nucleus is turned through an α_2 angle, so its nucleon distribution function is as follows:

$$\rho_2^{(0)}(\mathbf{r}) = \rho_0\left\{1 + \exp\left[\frac{r - \tilde{R}_2(\beta_2^{(2)}, \beta_3^{(2)}; \theta'_2)}{a}\right]\right\}^{-1}, \quad \text{(B.1)}$$

$$\tilde{R}_2(\beta_2^{(2)}, \beta_3^{(2)}; \theta'_2) = R_0^{(2)}\left(1 + \beta_2^{(2)} Y_{20}(\theta'_2) + \beta_3^{(2)} Y_{30}(\theta'_2)\right),$$

where ρ_0=0.17 fm^{-3},

$$\cos\theta'_2 = \cos\theta\cos(\pi - \alpha_2) + \sin\theta\sin(\pi - \alpha_2)\cos\phi\,. \quad \text{(B.2)}$$

The mass center of the projectile-nucleus is shifted to the end of the vector $\mathbf{R}$ and its symmetry axis is turned by the angle $\pi - \alpha_1$. According to the transformation formulae of the parallel transfer of vectors the variables of the transferred system O' are as follows:

$$r'^2 = r^2 + R^2 - 2rR\cos(\omega_{12}), \qquad \text{(B.3)}$$
$$\cos(\omega_{12}) = \cos\theta\cos\Theta + \sin\theta\sin\Theta\cos(\phi - \Phi),$$
$$\cos\theta'_1 = \frac{(r\cos\theta - R\cos\Theta)}{r'},$$
$$\cos\phi'_1 = (1 + \tan^2\phi'_1)^{-1/2},$$
$$\tan\phi'_1 = \frac{r\sin\phi\sin\theta - R\sin\Theta\sin\Phi}{r\cos\phi\sin\theta - R\sin\Theta\cos\Phi}.$$

In the coordinate system O', the deviation of the symmetry axis of projectile-nuclei relative to the $O'z'$ axis is determined by the angle

$$\cos\theta''_1 = \cos\theta'_1\cos(\pi - \alpha_1) + \sin\theta'_1\cos\phi'_1. \qquad \text{(B.4)}$$

Now the nucleon distribution function of the projectile-nucleus looks like

$$\rho_1^{(0)}(\mathbf{r}') = \rho_0\left\{1 + \exp\left[\frac{r' - \tilde{R}_1(\beta_2^{(1)}, \beta_3^{(1)}; \theta'_1)}{a}\right]\right\}^{-1}, \quad \text{(B.5)}$$

$$\tilde{R}_1(\beta_2^{(1)}, \beta_3^{(1)}; \theta'_1) = R_0^{(1)}\left(1 + \beta_2^{(1)} Y_{20}(\theta'_1) + \beta_3^{(1)} Y_{30}(\theta'_1)\right).$$

The nuclear part of the nucleus-nucleus potential was calculated by (A.3) using the folding procedure of the effective nucleon-nucleon forces by Migdal [22] with the nucleon distribution functions (B.1) and (B.5) of interacting nuclei.

References

1. S. Hofmann, Rep. Progr. Phys. **61**, 639 (1998); S. Hofmann et al., Z. Phys. A, **358**, 125 (1997) 125.
2. V.V. Volkov, N.A. Antonenko, E.A. Cherepanov, A.K. Nasirov, V.P. Permjakov, Phys. Lett. B **319**, 425 (1993); Phys. Rev. C **51**, 2635 (1995).
3. E.A. Cherepanov, V.V. Volkov, N.V. Antonenko, A.K. Nasirov, Nucl. Phys. A **459**, 145 (1996).
4. G.G.Adamian, N.V.Antonenko, W.Scheid, V.V.Volkov, Nucl. Phys. A **633**, 409 (1998).
5. G.G. Adamian, R.V. Jolos, A.I. Muminov, A.K. Nasirov, Phys. Rev. C **56**, 373 (1997).
6. A. D'Arrigo, G. Giardina, M. Herman, A.N. Ignatyuk, A. Taccone, J. Phys. G. **20**, 365 (1994).
7. A.H. Wapstra, G. Audi, Nucl. Phys. A **432**, 1 (1985).
8. P. Möller, J.R. Nix, At. Data Nucl. Data Tables **39**, 213 (1988).
9. O. Bohr, B. Mottelson, *Nuclear Structure*, Vols. I and II (Benjamin, New York, Amsterdam, 1975).
10. S.E. Vigdor, H.J. Karwowski, Phys. Rev. C **26**, 1068 (1982).
11. A. D'Arrigo, G. Giardina, M. Herman, A. Taccone, Phys. Rev. C **46**, 1437 (1992).
12. A. D'Arrigo, G. Giardina, M. Herman, M. Sacchi, A. Taccone, Phys. Lett. B **334**, 1 (1994).
13. A.V. Ignatyuk, G.N. Smirenkin, A.S. Tishin, Sov. J. Nucl. Phys. **21**, 255 (1975).

14. A.V. Ignatyuk, K.K. Istekov, G.N. Smirenkin, Sov. J. Nucl. Phys. **29**, 450 (1979).
15. A.J. Sierk, Phys. Rev. C **33**, 2039 (1986).
16. P. Grange, H.A. Weidenmüller, Phys. Lett. B **96**, 26 (1980).
17. E.M. Rastopchin, S.I. Mulgin, U.V. Ostapenko, V.V. Pashkeevich, M.I. Svirin, G.N. Smirenkin, Sov. J. Nucl. Phys. **53**, 741 (1991).
18. H.A. Kramers, Physica **7**, 284 (1940).
19. C. Bhattacharya, S. Bhattacharya, K. Krishan, Phys. Rev. C **53**, 1012 (1996).
20. V. Ninov et al., Phys. Rev. Lett. **83**, 1104 (1999).
21. C.Y. Wong, Phys. Rev. Lett. **31**, 766 (1973).
22. A.B. Migdal, *Theory of the Finite Fermi-Systems and Properties of Atomic Nuclei* (Moscow, Nauka, 1983).
23. S. Raman, C.H. Malarkey, W.T. Milner, C.W. Nestor Jr., P.H. Stelson, At. Data Nucl. Data Tables **36**, 1 (1987).
24. R.H. Spear, At. Data Nucl. Data Tables **42**, 55 (1989).
25. G.G. Adamian, A.K. Nasirov, N.V. Antonenko, R.V. Jolos, Phys. Part. Nucl. **25**, 583 (1994).
26. D. Pines, P. Noziéres, *Theory of Quantum Liquids* (Benjamin, New York, 1966).